

**Extended Supplemental Material: Vertex function compliant with
the Ward identity for quasiparticle self-consistent calculations
beyond GW**

Alexey Tal,^{1,*} Wei Chen,² and Alfredo Pasquarello¹

¹*Chaire de Simulation à l'Échelle Atomique (CSEA),*

Ecole Polytechnique Fédérale de Lausanne (EPFL), CH-1015 Lausanne, Switzerland

²*Institute of Condensed Matter and Nanoscience (IMCN),*

Université catholique de Louvain, B-1348 Louvain-la-Neuve, Belgium

* alexey.tal@epfl.ch

The present version of the supplemental material supersedes the version found on the web page of the journal (see Erratum). As the range-separated vertex has erroneously been described in Equation (5) of the supplemental material to the original paper (see Erratum), we provide the corrected expression in Section I. The results obtained with improved accuracy (higher NBANDSGW) compared to the results presented in the article are provided in Fig. 7 and Tables II, III, IV, and V.

The structure of this supplemental material is the following. Section I provides a detailed description of the vertex approximations. Section II describes the computational details and provides the convergence parameters. The extrapolation procedure used for correcting the results for the finite basis set is provided in Section III and the updated results are summarized in Section IV.

I. VERTEX CORRECTIONS

In reciprocal space the response function χ_0 is defined as follows

$$\chi_{0\mathbf{G},\mathbf{G}'}(\mathbf{q}, \omega) = \frac{1}{\Omega} \sum_{nn'\mathbf{k}} 2w_{\mathbf{k}} (f_{n'\mathbf{k}+\mathbf{q}} - f_{n'\mathbf{k}}) \times \frac{\langle \psi_{n'\mathbf{k}+\mathbf{q}} | e^{i(\mathbf{q}+\mathbf{G})\mathbf{r}} | \psi_{n\mathbf{k}} \rangle \langle \psi_{n\mathbf{k}} | e^{-i(\mathbf{q}+\mathbf{G}')\mathbf{r}'} | \psi_{n'\mathbf{k}+\mathbf{q}} \rangle}{\epsilon_{n'\mathbf{k}+\mathbf{q}} - \epsilon_{n\mathbf{k}} - \omega - i\eta}. \quad (1)$$

Here Ω is the volume of the system, $w_{\mathbf{k}}$ is the weight of the \mathbf{k} point, and the $f_{n\mathbf{k}}$ are the one electron occupancies of the states (n, \mathbf{k}) , η is a positive infinitesimal, the factor of 2 is due to the spin-degenerate systems considered here, and the band indices n and n' run over all the bands.

The behavior of Γ in $q \rightarrow 0, \omega \rightarrow 0$ limit is given by the first Ward identity, which connects the vertex and the renormalization factor $\Gamma = 1/Z$. Hence, we find a static xc kernel in the long-range limit

$$\lim_{\mathbf{q}+\mathbf{G}+\mathbf{G}' \rightarrow 0} \Gamma = \frac{1}{1 - f_{xc}^{00}(\mathbf{q} \rightarrow 0, \omega \rightarrow 0) \chi_0^{00}(\mathbf{q} \rightarrow 0, \omega \rightarrow 0)} = \frac{1}{Z(\mathbf{q} \rightarrow 0, \omega \rightarrow 0)}, \quad (2)$$

where the indices 00 indicate the head of the matrix. Considering that f_{xc}^{00} and χ_0^{00} are scalar functions, we find the static long-range xc kernel

$$f_{xc}^{\text{LR}}(\mathbf{q} \rightarrow 0, \omega \rightarrow 0) = \frac{1 - Z(\mathbf{q} \rightarrow 0, \omega \rightarrow 0)}{\chi_0^{00}(\mathbf{q} \rightarrow 0, \omega \rightarrow 0)}. \quad (3)$$

The ALDA kernel in reciprocal space is obtained via the Fourier transform

$$f_{xc,\mathbf{G},\mathbf{G}'}^{\text{LDA}} = \frac{1}{\Omega} \int_{\Omega} d\mathbf{r} e^{-i(\mathbf{G}-\mathbf{G}') \cdot \mathbf{r}} f_{xc} [n(\mathbf{r})], \quad (4)$$

where, Ω is the volume of the unit cell.

The vertex of the $QSGW$ scheme reads

for $\mathbf{G} = \mathbf{G}'$:

$$f_{xc,\mathbf{G},\mathbf{G}}^{\text{LR+LDA}}(\mathbf{q}, \omega) = \frac{1 - Z(\mathbf{q} = 0, \omega = 0)}{\chi_0^{00}(\mathbf{q}, \omega = 0)} e^{-|\mathbf{q} + \mathbf{G}|^2/k_{\text{TF}}^2} + f_{xc,\mathbf{G},\mathbf{G}'}^{\text{LDA}}(1 - e^{-|\mathbf{q} + \mathbf{G}|^2/k_{\text{TF}}^2}), \quad (5)$$

and for $\mathbf{G} \neq \mathbf{G}'$:

$$f_{xc,\mathbf{G},\mathbf{G}'}^{\text{LR+LDA}}(\mathbf{q}, \omega) = f_{xc,\mathbf{G},\mathbf{G}'}^{\text{LDA}}(1 - \delta_{\mathbf{G},0})(1 - \delta_{0,\mathbf{G}'}) \quad (6)$$

II. COMPUTATIONAL DETAILS

The calculations are performed with the projector augmented wave (PAW) method [1] implemented in VASP [2, 3]. $QSGW$ calculations with the nanoquanta vertex corrections are performed starting with G_0W_0 energies, wave functions, and dielectric matrices. All other $QSGW$ calculations are performed starting from PBE. To achieve convergence, six iterations are performed. The derivative of the cell-periodic part of the orbitals w.r.t. the \mathbf{k} -points is calculated with the PEAD method [4].

The Al_sv_GW, O_GW_new, As_d, N_GW_new, P_GW, Ar_GW, B_GW, C_GW_new, Ca_sv_GW, Cd_sv_GW, S_GW, Se_sv_GW, Ga_d_GW, Ge_d_GW, In_d_GW, Li_sv_GW, Cl_GW, F_GW_new, Mg_sv_GW, Si_sv_GW, and Zn_sv_GW ultrasoft PAW (US-PAW) potentials are used in the calculations. The semicore states are included in the case of (post-)transition metals.

In order to correct the d -band positions calculated with US-PAW, we apply the shift

$$\Delta = \varepsilon_d^{GW^{\text{NQ}}} [\text{US} - \text{PAW}] - \varepsilon_d^{GW^{\text{NQ}}} [\text{NC} - \text{PAW}],$$

where the values for $\varepsilon_d^{GW^{\text{NQ}}} [\text{NC} - \text{PAW}]$ are taken from Ref. [5]. The corrections Δ are given in Table V.

The Thomas-Fermi vector is calculated as a macroscopic average of the electron density over the unit cell. In the transition metals, d electrons are included in the valence which can lead to an overestimation of k_{TF} in such systems.

TABLE I. Convergence parameters and structures used in the calculations. The structures are the same as in Ref. [6]. Z is the converged renormalization factor corresponding to the VBM.

	$E_{\text{cutoff}}^{\text{DFT}}$ (eV)	$E_{\text{cutoff}}^{\text{GW}}$ (eV)	N_ω	N_{empty}	N_{updated}	k-points	Space group	$a_0(\text{\AA})$	c_0/a_0	Z
AlAs	500	333	150	512	64	$6 \times 6 \times 6$	$F\bar{4}3m$	5.661		0.79
AlP	500	333	110	512	64	$6 \times 6 \times 6$	$F\bar{4}3m$	5.451		0.79
Ar	600	400	90	1024	64	$6 \times 6 \times 6$	$Fm\bar{3}m$	5.26		0.89
BN	500	333	110	512	64	$6 \times 6 \times 6$	$F\bar{4}3m$	3.616		0.84
C	500	333	50	512	64	$6 \times 6 \times 6$	$Fd\bar{3}m$	3.567		0.84
CaO	400	266	110	256	64	$6 \times 6 \times 6$	$Fm\bar{3}m$	4.803		0.81
CdS	500	333	150	512	64	$6 \times 6 \times 6$	$F\bar{4}3m$	5.818		0.79
CdSe	500	333	150	512	64	$6 \times 6 \times 6$	$F\bar{4}3m$	6.052		0.79
GaAs	500	333	130	1024	64	$6 \times 6 \times 6$	$F\bar{4}3m$	5.648		0.80
GaN	500	333	70	1024	64	$6 \times 6 \times 6$	$P6_3mc$	3.189	1.626	0.80
GaP	500	333	90	1024	64	$6 \times 6 \times 6$	$F\bar{4}3m$	5.448		0.78
InP	500	333	150	512	64	$6 \times 6 \times 6$	$F\bar{4}3m$	5.866		0.77
LiCl	500	333	70	512	64	$6 \times 6 \times 6$	$Fm\bar{3}m$	5.106		0.85
LiF	600	400	50	1024	64	$6 \times 6 \times 6$	$Fm\bar{3}m$	4.010		0.87
MgO	500	333	130	512	64	$6 \times 6 \times 6$	$Fm\bar{3}m$	4.207		0.83
Si	600	400	128	512	64	$6 \times 6 \times 6$	$Fd\bar{3}m$	5.430		0.77
SiC	600	400	110	512	64	$6 \times 6 \times 6$	$F\bar{4}3m$	4.358		0.82
ZnO	500	333	200	1024	64	$4 \times 4 \times 4$	$P6_3mc$	3.250	1.601	0.92
ZnS	500	333	150	512	64	$6 \times 6 \times 6$	$F\bar{4}3m$	5.410		0.80
ZnSe	500	333	150	512	64	$6 \times 6 \times 6$	$F\bar{4}3m$	5.667		0.81

III. CONVERGENCE

The convergence parameters of the calculations are provided in Table I. The calculated bands are corrected for the finite basis set through the extrapolation scheme described in Ref. [7]. For the extrapolations shown in Figs. 1 and 2, we increase the default energy cutoff by up to a factor of two to achieve a better convergence with the number of empty bands. However, as shown in Fig. 4, in the presence of the LDA vertex function in the self-energy, the convergence of the QP energies with the number of empty bands deviates from the linear trend, which is attributed to the limited accuracy of the US-PAW potentials for energies beyond 10–20 Ry above the vacuum level [7]. As shown in Fig. 6, the improved description of the empty states results in an extension of the linear region. Hence, for the case of $\text{QSG}\hat{W}$, the extrapolation is performed in two steps. In the first step, the QP energy values are found by a linear extrapolation based on the calculations with a reduced set of unoccupied

bands, where the energies of the states are below 20 Ry and the potentials are accurate. In the second step, we correct for this reduced set of bands by adding the difference between the full and the reduced set of bands as achieved with the $\text{QSG}\tilde{W}^{\text{LR}}$ scheme (see Fig. 5).

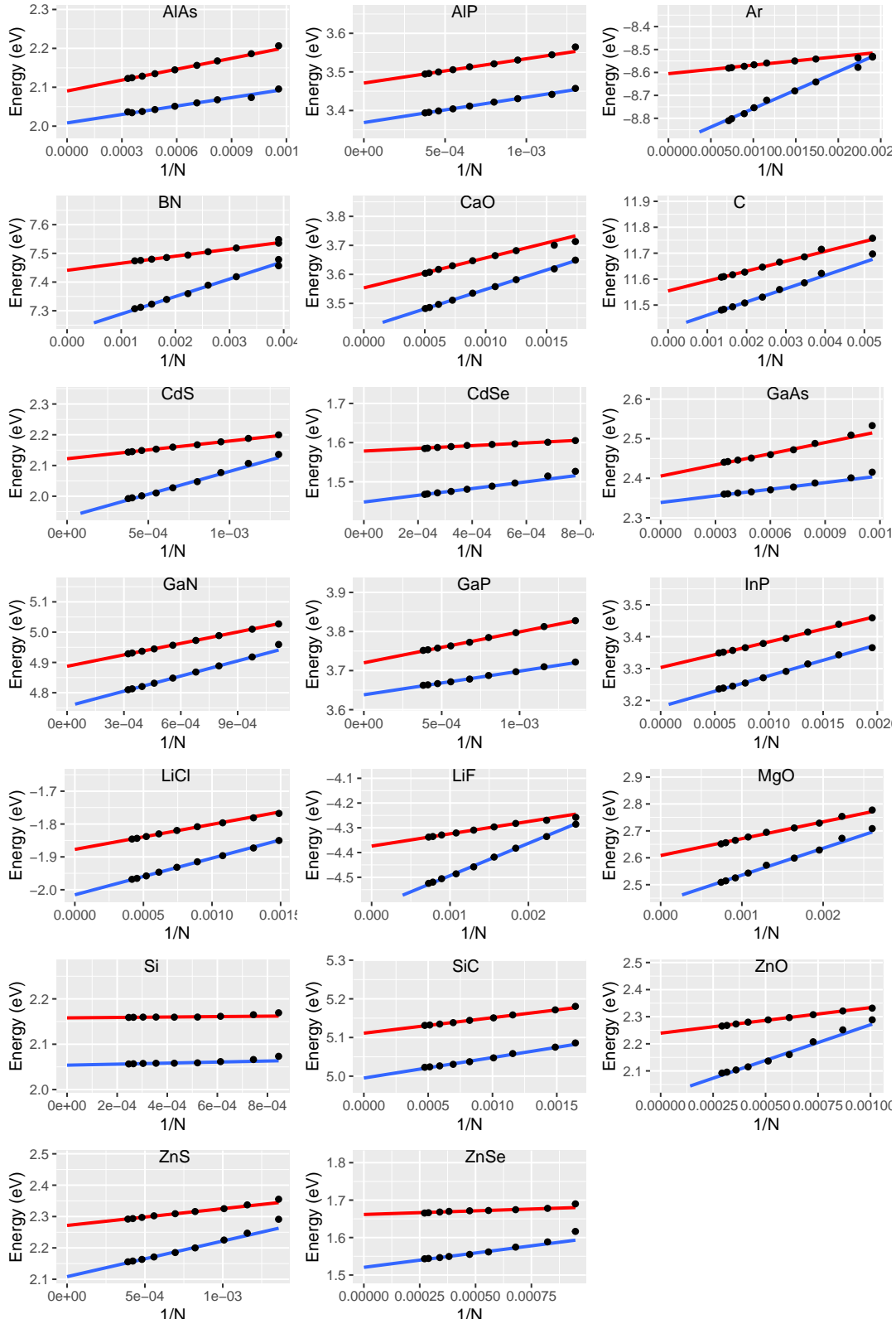


FIG. 1. Extrapolation of the VBM (blue) and CBM (red) with the inverse of the number of unoccupied bands calculated in the QSGW approximation. The absolute values of the VBM are shifted.

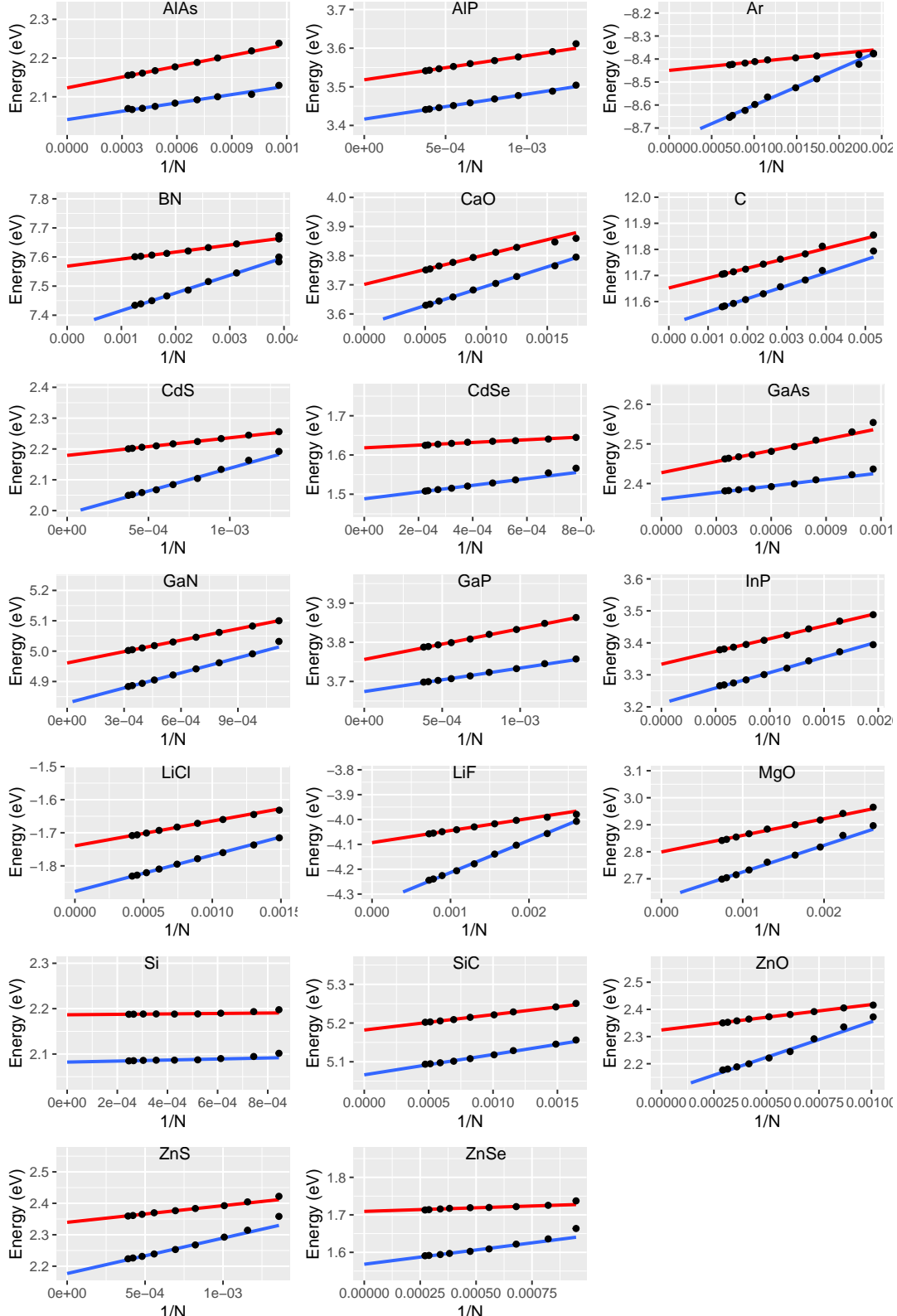


FIG. 2. Extrapolation of the VBM (blue) and CBM (red) with the inverse of the number of unoccupied bands calculated in the QSGW^{LR} approximation. The absolute values of the VBM are shifted.

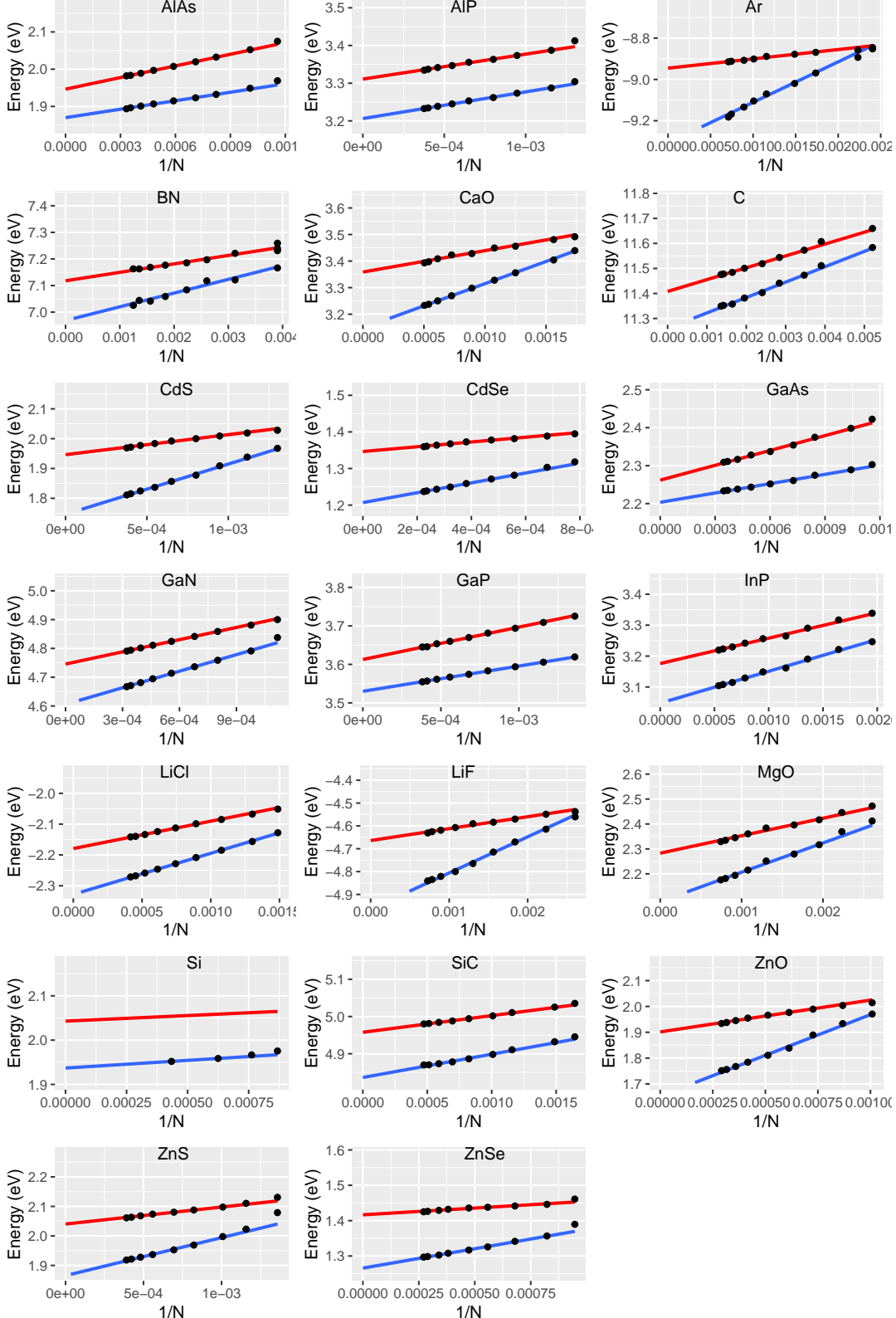


FIG. 3. Extrapolation of the VBM (blue) and CBM (red) with the inverse of the number of unoccupied bands calculated in the $\text{QSG}\tilde{W}^{\text{NQ}}$ approximation. The absolute values of the VBM are shifted.

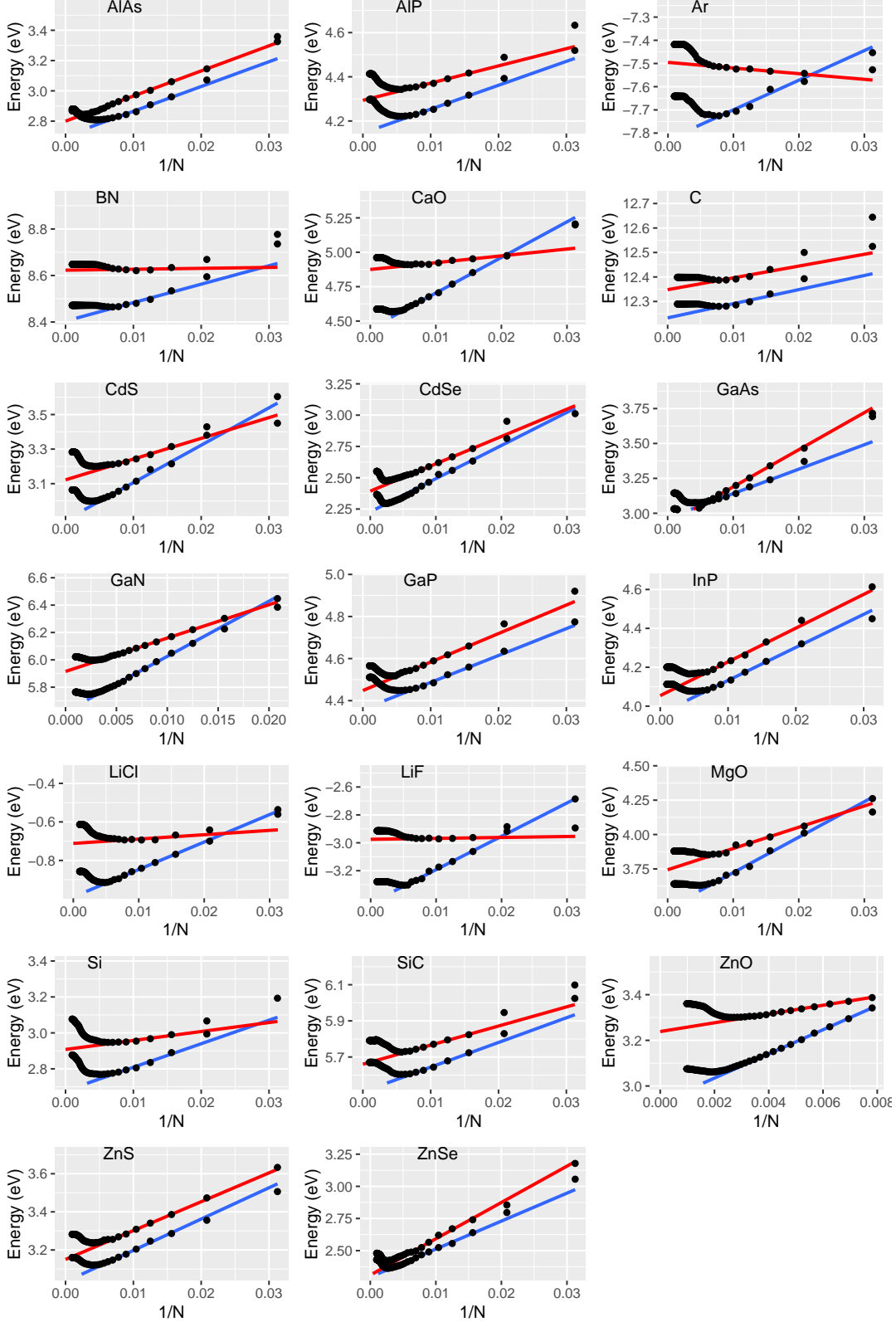


FIG. 4. Extrapolation of the VBM (blue) and CBM (red) with the inverse of the number of unoccupied bands calculated in the $QSG\hat{W}$ approximation. The absolute values of the VBM are shifted.

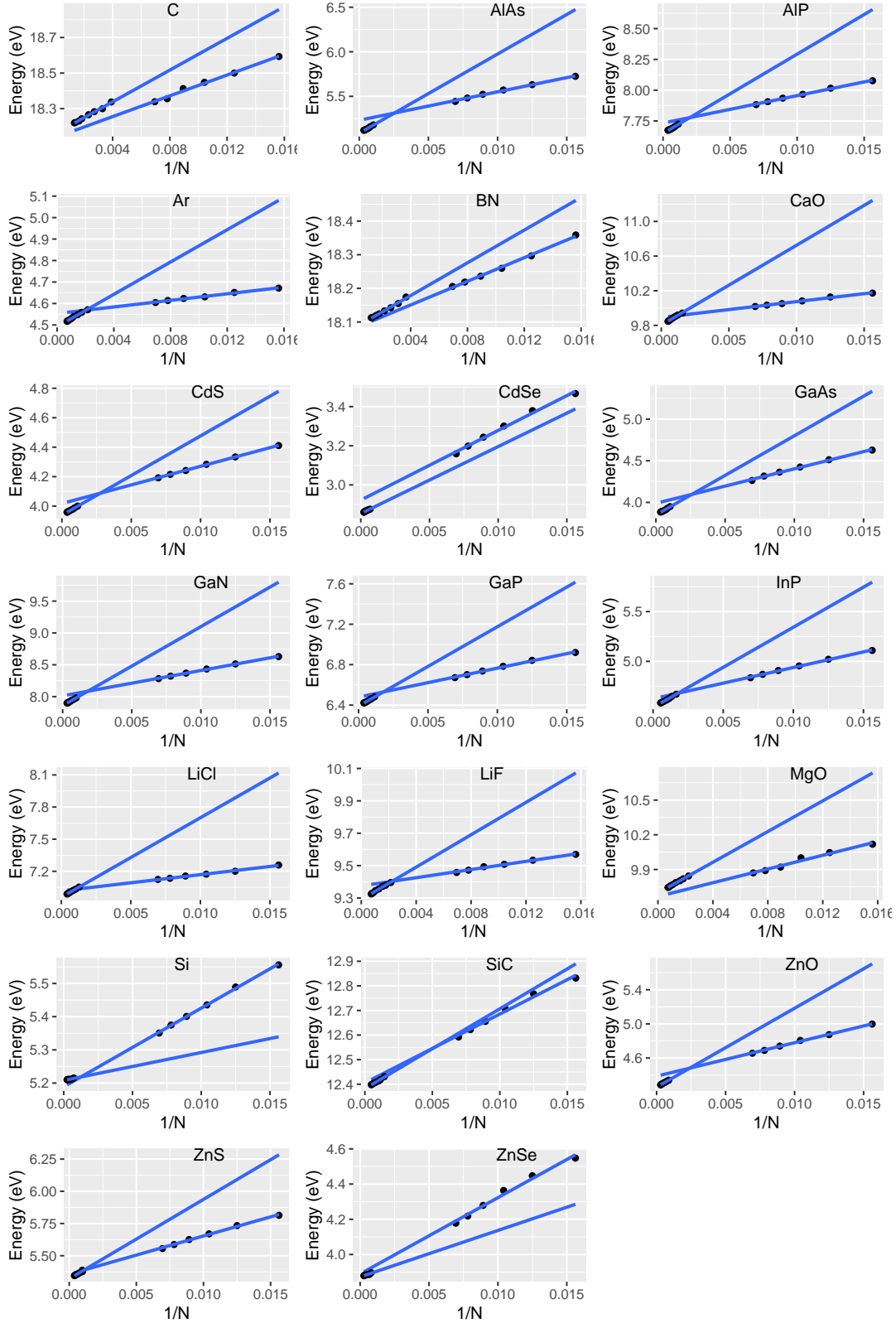


FIG. 5. Extrapolations of the VBM with the inverse of the number of unoccupied bands calculated in the QSGW^{LR} approximation. The two lines correspond to the extrapolation achieved with the reduced number of bands and with the extrapolation to the infinite basis set limit.

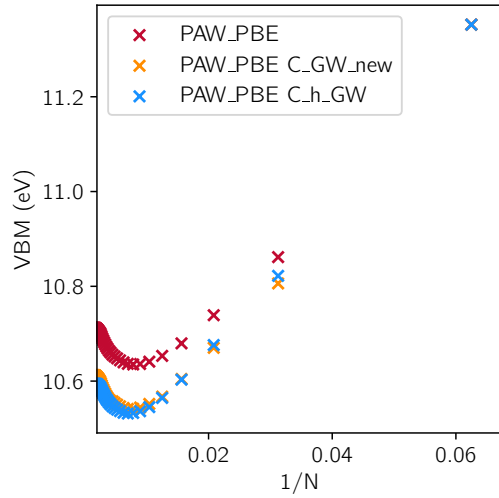


FIG. 6. The convergence of the VBM of diamond with the number of empty bands for three PAW potentials. PAW_PBE are standard PAW potentials for DFT calculations, PAW_PBE C_GW_new are standard PAW potentials for GW calculations, and PAW_PBE C_h_GW are PAW potentials matching the quality of norm-conserving ones for GW calculations. For clarity, the values of PAW_PBE and PAW_PBE C_GW_new are shifted to match PAW_PBE C_h_GW in the point at lowest N .

IV. RESULTS

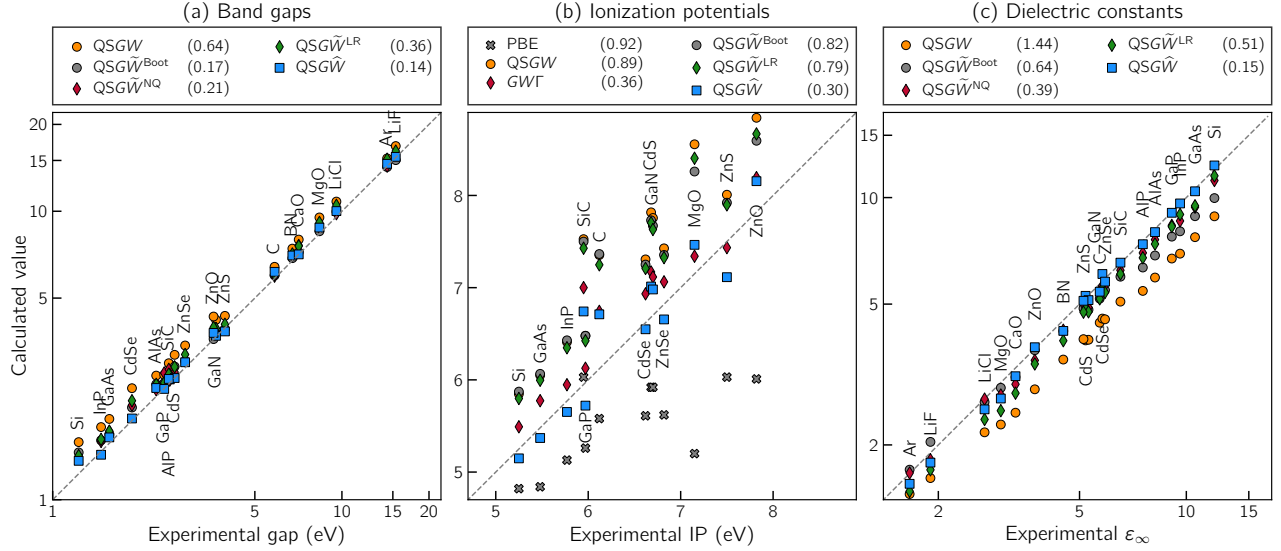


FIG. 7. Results of the QSGW calculations with various vertex corrections. The corresponding mean absolute errors (MAEs) are given in the legends (energies in eV). In (a) and (c), the band gaps and the dielectric constants are plotted on a logarithmic scale. Zero-point electron-phonon renormalizations are taken into account by modifying the experimental values. In (b), the first ionization potentials obtained with Perdew-Burke-Ernzerhof PBE and GWT are taken from Ref. [5]. The IPs are calculated as QP shifts added to the PBE values from Ref. [5]. We take the average value for the experimental IP when multiple references are available. In (c), the dielectric constants are obtained from the RPA and the test-charge test-charge dielectric function.

TABLE II. Calculated band gaps (in eV). Experimental band gaps and zero-phonon renormalizaton (ZPR) corrections are taken from Ref. [6].

	QSGW	$\text{QSG}\tilde{W}^{\text{Boot}}$	$\text{QSG}\tilde{W}^{\text{NQ}}$	$\text{QSG}\tilde{W}^{\text{LR}}$	$\text{QSG}\hat{W}$	Expt.+ZPR
AlAs	2.69	2.51	2.41	2.51	2.42	2.28
AlP	2.94	2.72	2.60	2.72	2.62	2.54
Ar	15.25	14.23	14.33	15.15	14.61	14.33
BN	7.42	6.88	7.02	7.11	7.03	6.74
C	6.42	5.99	5.96	6.04	6.17	5.85
CaO	7.98	7.21	7.61	7.57	7.09	7.09
CdS	3.18	2.90	2.77	2.89	2.65	2.64
CdSe	2.44	2.09	2.13	2.20	1.95	1.88
GaAs	1.91	1.68	1.72	1.73	1.61	1.57
GaN	4.20	3.77	3.81	3.93	3.72	3.67
GaP	2.71	2.54	2.75	2.54	2.44	2.43
InP	1.79	1.61	1.59	1.62	1.44	1.47
LiCl	10.80	9.97	9.81	10.49	10.03	9.57
LiF	16.83	15.04	15.75	16.16	15.43	15.35
MgO	9.52	8.52	8.78	9.14	8.77	8.36
Si	1.58	1.46	1.41	1.42	1.37	1.23
SiC	2.97	2.69	2.83	2.72	2.64	2.52
ZnO	4.32	3.60	3.80	3.95	3.79	3.60
ZnS	4.34	3.90	3.91	4.06	3.85	3.94
ZnSe	3.43	3.03	3.04	3.19	2.94	2.87
MAE	0.64	0.17	0.21	0.36	0.14	
ME	0.64	0.12	0.21	0.36	0.13	
MAPE	0.16	0.05	0.06	0.08	0.03	

TABLE III. Ionization potentials (in eV). The ionization potentials are obtained as a QP correction to the PBE values taken from Ref. [5]. MAEs are calculated relative to the average experimental value when several references are available. Experimental values are taken from Refs. [8–10].

	PBE ^a	HSE ^a	<i>GWT</i> ^a	QSGW	$\text{QSG}\tilde{W}^{\text{Boot}}$	$\text{QSG}\tilde{W}^{\text{LR}}$	$\text{QSG}\hat{W}$	Expt.
AlAs	5.32	5.83	6.37	6.73	6.73	6.65	5.87	
AlP	5.70	6.22	6.64	7.10	7.09	7.01	6.26	
BN	7.03	7.85	8.52	9.23	9.14	9.13	8.39	
C	5.58	6.18	6.74	7.35	7.36	7.25	6.69	6.12
CdS	5.92	6.60	7.17	7.82	7.73	7.70	6.99	6.68
CdSe	5.61	6.23	6.93	7.31	7.25	7.21	6.53	6.62
GaAs	4.84	5.32	5.77	6.05	6.07	6.00	5.35	5.48
GaN	5.92	6.61	7.12	7.76	7.67	7.63	7.00	6.70
GaP	5.26	5.75	6.13	6.48	6.48	6.42	5.71	5.97
InP	5.13	5.59	5.95	6.41	6.43	6.35	5.65	5.77
MgO	5.20	6.15	7.34	8.55	8.26	8.40	7.46	7.15
Si	4.82	5.22	5.49	5.85	5.87	5.80	5.12	5.25
SiC	6.03	6.64	7.00	7.53	7.50	7.43	6.72	5.95
ZnO	6.01	7.11	8.19	8.84	8.59	8.67	8.16	7.82
ZnS	6.03	6.77	7.43	8.01	7.92	7.90	7.13	7.50
ZnSe	5.62	6.29	7.06	7.43	7.35	7.33	6.63	6.82
MAE	0.92	0.37	0.36	0.89	0.82	0.79	0.30	
ME	-0.91	-0.26	0.35	0.89	0.82	0.79	0.10	
MAPE	0.14	0.06	0.06	0.14	0.13	0.12	0.05	

^a from Ref. [5]

TABLE IV. Calculated dielectric constants. Experimental values are taken from Ref. [6].

	$QSGW$	$QSG\tilde{W}^{\text{Boot}}$	$QSG\tilde{W}^{\text{LR}}$	$QSG\tilde{W}^{\text{NQ}}$	$QSG\hat{W}$	Expt.
AlAs	5.94	6.86	7.39	7.61	7.99	8.16
AlP	5.45	6.34	6.76	6.98	7.38	7.54
Ar	1.45	1.70	1.48	1.67	1.55	1.66
BN	3.49	4.20	3.94	4.22	4.20	4.50
C	4.43	5.18	5.17	5.40	5.42	5.70
CaO	2.47	3.11	2.80	2.97	3.13	3.30
CdS	3.95	4.83	4.87	5.02	5.28	5.20
CdSe	4.55	5.54	5.53	5.64	6.08	5.80
GaAs	7.73	8.86	9.48	9.40	10.42	10.58
GaN	3.96	4.82	4.76	4.89	5.13	5.30
GaP	6.73	7.76	8.28	8.35	9.06	9.10
InP	6.94	8.03	8.96	8.59	9.63	9.60
LiCl	2.17	2.64	2.36	2.69	2.52	2.70
LiF	1.61	2.04	1.70	1.82	1.78	1.90
MgO	2.28	2.90	2.50	2.77	2.71	3.00
Si	8.85	9.97	11.52	11.18	12.33	12.00
SiC	5.08	5.98	6.08	6.23	6.55	6.52
ZnO	2.87	3.70	3.39	3.47	3.78	3.74
ZnS	3.98	4.86	4.74	5.00	5.11	5.13
ZnSe	4.53	5.48	5.39	5.65	5.79	5.90
MAE	1.44	0.64	0.51	0.39	0.15	
ME	1.44	0.64	0.51	0.39	0.15	
MAPE	0.23	0.09	0.10	0.06	0.03	

TABLE V. Mean position (in eV) of the semicore d states at the Γ point with respect to the VBM. The experimental values and the values calculated with the NC-PAW potentials are taken from Ref. [5].

	NC-PAW		US-PAW				Δ	Expt.
	$GW\Gamma$	$G\tilde{W}^{NQ}$	$QSG\tilde{W}^{NQ}$	$QSGW$	$QSG\tilde{W}^{LR}$	$QSG\hat{W}$		
CdS	9.50	9.10	8.96	9.44	9.25	9.36	0.14	9.50
CdSe	9.70	9.20	9.13	9.48	9.36	9.45	0.07	10.04
GaAs	18.50	18.00	17.30	18.33	18.19	18.37	0.70	18.80
GaN	17.00	16.60	15.99	17.15	17.03	17.15	0.61	17.00
GaP	18.30	17.80	16.80	18.46	18.27	18.45	1.00	18.55
InP	16.90	16.30	16.69	16.57	16.41	16.61	-0.39	16.80
ZnO	7.10	6.90	6.49	7.23	7.14	7.01	0.41	7.50
ZnS	8.40	8.00	7.83	8.33	8.18	8.17	0.17	9.00
ZnSe	8.60	8.20	8.02	8.57	8.43	8.39	0.18	9.20
MAE	0.29	0.70	1.02	0.35	0.46	0.41		
ME	-0.27	-0.70	-1.02	-0.31	-0.46	-0.38		
MAPE	0.03	0.06	0.09	0.03	0.04	0.04		

-
- [1] P. E. Blöchl, Projector augmented-wave method, Phys. Rev. B **50**, 17953 (1994).
 - [2] G. Kresse and J. Hafner, Ab initio molecular dynamics for liquid metals, Phys. Rev. B **47**, 558 (1993).
 - [3] G. Kresse and J. Furthmüller, Efficient iterative schemes for ab initio total-energy calculations using a plane-wave basis set, Phys. Rev. B **54**, 11169 (1996).
 - [4] R. W. Nunes and X. Gonze, Berry-phase treatment of the homogeneous electric field perturbation in insulators, Phys. Rev. B **63**, 155107 (2001).
 - [5] A. Grüneis, G. Kresse, Y. Hinuma, and F. Oba, Ionization potentials of solids: The importance of vertex corrections, Phys. Rev. Lett. **112**, 096401 (2014).
 - [6] W. Chen, G. Miceli, G. M. Rignanese, and A. Pasquarello, Nonempirical dielectric-dependent hybrid functional with range separation for semiconductors and insulators, Phys. Rev. Mater. **2**, 073803 (2018).
 - [7] J. Klimeš, M. Kaltak, and G. Kresse, Predictive GW calculations using plane waves and pseudopotentials, Phys. Rev. B **90**, 075125 (2014).
 - [8] W. Mönch, *Semiconductor Surfaces and Interfaces*, edited by G. Ertl, R. Gomer, H. Lüth, and D. L. Mills, Springer Series in Surface Sciences, Vol. 26 (Berlin, Heidelberg, 2001).
 - [9] T. Jaouen, G. Jézéquel, G. Delhaye, B. Lépine, P. Turban, and P. Schieffer, Work function shifts, Schottky barrier height, and ionization potential determination of thin MgO films on Ag(001), Appl. Phys. Lett. **97**, 232104 (2010).
 - [10] A. Facchetti and T. J. Marks, eds., *Transparent Electronics: From Synthesis to Applications* (Chichester, UK, 2010).